Determinants of Spike Infectivity, Processing and Neutralization in SARS-CoV-2 Omicron subvariants BA.1 and BA.2

Chiara Pastorio[1#], Fabian Zech[1#], Sabrina Noettger[1], Christoph Jung[2], Timo Jacob[2], Konstantin M.J. Sparrer[1] and Frank Kirchhoff[1*]

[1] Institute for Molecular Virology
Ulm University Medical Centre
89081 Ulm, Germany

[2] Institute of Electrochemistry
Ulm University
89081 Ulm, Germany

# both contributed equally and are in alphabetical order

* Correspondence: Frank.Kirchhoff@uni-ulm.de

Running title: Functional impact of the Omicron Spike mutations

KEYWORDS: SARS-CoV-2, Omicron, Spike protein, COVID-19, neutralization, BA.1, BA.2, variant evolution

ABSTRACT

The SARS-CoV-2 Omicron variant rapidly outcompeted other variants and currently dominates the COVID-19 pandemic. Its enhanced transmission, immune evasion and pathogenicity is thought to be driven by numerous mutations in the Omicron Spike protein. Here, we examined the impact of amino acid changes that are characteristic for the BA.1 and/or BA.2 Omicron lineages on Spike function, processing and susceptibility to neutralization. Individual mutations of S371F/L, S375F and T376A in the ACE2 receptor-binding domain as well as Q954H and N969K in the hinge region 1 impaired infectivity, while changes of G339D, D614G, N764K and L981F moderately enhanced it. Most mutations in the N-terminal region and the receptor binding domain reduced sensitivity of the Spike protein to neutralization by sera from individuals vaccinated with the BNT162b2 vaccine or therapeutic antibodies. Our results represent a systematic functional analysis of Omicron Spike adaptations that allowed this SARS-CoV-2 variant to overtake the current pandemic.

HIGHLIGHTS

- S371F/L, S373P and S375F impair Spike function and revert in some BA.1 isolates
- Changes of Q954H and N969K in HR1 reduce while L981F enhances S-mediated infection
- Omicron-specific mutations in the NTD and RBD of Spike reduce neutralization
- N440K, G446S, E484A and Q493K confer resistance to bamlanivimab or imdevimab

INTRODUCTION

SARS-CoV-2, the causative agent of the Coronavirus disease 2019 (COVID-19) pandemic, has infected more than 500 million people around the globe and caused almost 6.2 million fatalities (https://coronavirus.jhu.edu/map.html; April 13th, 2022). Effective vaccination is the best way to get this devastating pandemic under control. A variety of safe and effective vaccines against SARS-CoV-2 are available and more than 10 billion vaccine doses have been administered to date. However, low access to, or acceptance of vaccines together with the emergence of new SARS-CoV-2 variants jeopardise this strategy. So called variants of concern (VOCs) pose a particular risk. Their increased transmissibility, efficient immune evasion and altered pathogenicity are mainly determined by the viral spike (S) protein (Harvey et al., 2021; Jung et al., 2022; Tao et al., 2021).

Currently, the fifth SARS-CoV-2 VOC, termed Omicron, dominates the COVID-19 pandemic. The Omicron VOC was first detected in Botswana and South Africa in November 2021 and outcompeted the Delta VOC in an amazingly short time. Evolutionary studies revealed that the Omicron VOC evolved independently, possibly in a chronically infected immunocompromised individual, human population under poor surveillance or an unknown non-human species from which it spilled back to humans (Karim et al., 2021; Wei et al., 2021). Omicron contains a strikingly high number of mutations (Jung et al., 2022), especially in its S protein, compared to other variants and the initial Wuhan strains. Recent studies support that this VOC is highly transmissible and shows an increased ability to infect convalescent and vaccinated individuals (Altarawneh et al., 2022; Espenhain et al., 2021; Grabowski et al., 2022; Pulliam et al., 2022). This agrees with the finding that the Omicron VOC shows reduced susceptibility to neutralizing antibodies induced by previous SARS-CoV-2 infection or vaccination (Andrews et al., 2021; Cele et al., 2021; Hoffmann et al., 2021; Lu et al., 2021; Planas et al., 2021; Wilhelm et al., 2021). Notably, accumulating evidence suggests that Omicron infections are associated

with milder symptoms and decreased hospitalization and fatality rates compared to infections with the Delta SARS-CoV-2 VOC (Moore and Baden, 2022; Wolter et al., 2022).

The SARS-CoV-2 S protein is the major membrane glycoprotein required for recognising the viral receptor angiotensin-converting enzyme 2 (ACE2) and subsequent entry into target cells (Hoffmann et al., 2020; Letko et al., 2020). Thus, the S protein critically determines the cell tropism and transmissibility of SARS-CoV-2 in human populations. To mediate attachment and fusion, the S precursor needs to be proteolytically processed by cellular proteases after synthesis. The proprotein convertase furin cleaves S at the S1/S2 site to generate the S1 subunit, which is responsible for receptor binding, while the transmembrane serine protease 2 (TMPRSS2) or cathepsins B and L cleave at the S2′ site just upstream of the hydrophobic fusion peptide to release the S2 subunit mediating membrane fusion (Walls et al., 2020; Wrapp et al., 2020). In its active form the S protein of SARS-CoV-2 forms trimers on the surface of the viral particles. Consequently, the S protein is also the major target of protective humoral immune responses (Walls et al., 2020) and all COVID-19 vaccines are based on the SARS-CoV-2 S antigen. Thus, mutations in the N-terminal or receptor binding domains (NTD and RBD, respectively) of S can confer increased resistance to neutralizing antibodies (Dai and Gao, 2021). It is clear that alterations in the viral surface glycoprotein Spike (S) of the Omicron VOC play a key role in its high transmissibility, efficient immune evasion and reduced pathogenicity. However, the impact of most amino acid changes distinguishing the Omicron S protein from that of the original Wuhan SARS-CoV-2 strain on viral infectivity and susceptibility to neutralization remains to be determined.

Here, we analyzed the functional impact of individual amino acid changes that distinguish the dominant 21K (BA.1) Omicron VOC and the emerging 21L (BA.2) variant from the early 2020 Wuhan SARS-CoV-2 isolate. To achieve this, we introduced a total of 48 mutations in the S protein of the Wuhan strain and determined their impact on viral infectivity, expression and

proteolytic processing, as well as susceptibility to neutralizing antibodies and sera from vaccinated individuals. We show that several amino acid changes found in the Omicron S protein impair infectivity and demonstrate that numerous alterations in the NTD and RBD of BA.1 and or BA.2 S proteins affect neutralization by sera from BNT/BNT vaccinated individuals and therapeutic antibodies.

RESULTS

Generation of S Proteins containing mutations found in Omicron

Omicron is currently classified into two major lineages, BA.1 (21K) and BA.2 (21L) (Figure 1A) (Hadfield et al., 2018; Sagulenko et al., 2018). BA.1 has replaced the Delta VOC and dominated the COVID-19 pandemic at the beginning of 2022 (Figure 1B). However, the frequency of the BA.2 lineage is increasing (Figure 1B) and this variant has outcompeted BA.1 in many countries, such as India, Denmark, Austria and South Africa (Viana et al., 2022). Although only ~13% of the SARS-CoV-2 genome encodes for the S protein, this region contains most mutations distinguishing the Omicron VOCs from the original Wuhan Hu-1 SARS-CoV-2 strain. Many of the mutations that distinguish the Omicron S proteins from those of other SARS-CoV-2 variants are located in the RBD that interacts with the viral ACE2 receptor and is a major target of neutralizing antibodies (Figure 1C). The Omicron BA.1 and BA.2 S proteins share about 20 amino acid changes in S compared to the 2020 Wuhan Hu-1 strain and 12 of these are located in the RBD (Figures 1C, 1D). In the consensus, a total of 14 mutations are specific for BA.1 and 9 for BA.2 (Figures 1C, 1D). Thirteen of the 23 S consensus lineage-specific variations are located in the NTD (Figure 1D). All 43 non-synonymous defining mutations, insertions and deletions found in BA.1 and BA.2 Omicron VOCs (https://covariants.org/variants/21L) were introduced individually in the S protein of the original Wuhan Hu-1 strain by site-directed mutagenesis. Sequence analysis of the full-length S genes verified that all constructs contained the desired mutations (Figure 1D) and confirmed the absence of additional changes.

116 **Impact of mutations in Omicron Spike on viral pseudoparticle infection**

117 To analyse the functional impact of mutations found in the Omicron BA.1 and BA.2 variants,
118 we generated vesicular stomatitis virus (VSV) particles pseudotyped with the parental and
119 mutant SARS-CoV-2 S proteins. Previous studies established that these VSV pseudoparticles
120 (VSVpp) mimic key features of SARS-CoV-2 entry, such as receptor usage, cell tropism,
121 protease dependency and susceptibility to neutralizing antibodies (Hoffmann et al., 2020; Riepler
122 et al., 2020; Schmidt et al., 2016). We found that the BA.1 S showed moderately reduced and
123 the BA.2 S slightly enhanced infection efficiencies compared to the Wuhan Hu-1 S, while the S
124 protein of the Delta VOC did not differ significantly from the original form (Figure 2A, left).
125 Most of the 20 amino acid changes in S that are shared between the BA.1 and BA.2 variants did
126 not significantly affect the efficiency of VSVpp infection (Figures 2A; S1). In agreement with
127 previous findings (Korber et al., 2020; Yurkovetskiy et al., 2020), substitution of D614G slightly
128 enhanced infection. Similarly, mutations of G339D, K417N and N764K had subtle enhancing
129 effects. Notably, modest enhancing effects were not due to saturation of infection since only up
130 to 10% of all target cells became GFP positive during the single round of infection (Figure S1).
131 Substitution of S375F in the RBD drastically impaired and mutations of Q954H and N969K in
132 HR1 reduced VSVpp infectivity (Figure 2A; S1).

133 Most of the BA.1 and BA.2 specific variations in the NTD of the S protein had minor effects
134 on VSVpp infectivity (Figure 2A). Three changes (Δ69-70, T95I and L212I) in the NTD slightly
135 enhanced and six alterations (T19I, Δ24-26, A67V, Δ142-144, Y145D, and Δ211) reduced
136 VSVpp infection. Similar to the shared S375F, mutations of S371L or S371F in the BA.1 and
137 BA.2 S proteins, respectively, strongly impaired viral infectivity. The adjacent BA.2-specific
138 T376A change had similar disruptive effects (Figure 2A). Mutation of N856K that is specific for
139 BA.1 and might stabilize the fusion peptide proximal region (Zhang et al., 2022) and T19I or

Δ24-26 near the N-terminus of BA.2 S markedly reduced VSVpp infection (Figure 2A), although these residues do not affect known functional domains.

To assess infection kinetics and to challenge the above-mentioned infection results, we performed assays allowing automated quantification of the number of VSVpp infected (GFP+) Caco-2 cells over time. The various mutant S proteins mediated infection with similar kinetics but varying and frequently reduced efficiencies (Figure 2B). The results confirmed that the BA.1 S shows moderately diminished infection efficiency compared to the Hu-1 Wuhan S protein. Individual mutations of T19I, Δ24-26, A67V, Y145D, S371L, S371F, S373P, S375F, T376A, G446S, Q493R, G496S, N679K, P681H, D796Y, N856K, Q954H and N969K all reduced the activity of the Hu-1 S to levels similar or below that obtained for the BA.1 S protein (Figure 2B). In contrast, shared mutations of N440K and D614G, as well as BA.1-specific changes of Δ69-70, Δ211, insertion of 214EPE, and mutation of L981F increased infection efficiencies. Our results agree with recent findings suggesting that the Q954H and N969K changes in heptad repeat 1 (HR1) reduce rather than enhance fusion efficiency (Suzuki et al., 2022; Xia et al., 2022; Zhao et al., 2021). In addition, our analysis revealed that N856K in BA.1 S and T19I as well as Δ24-26 in the BA.2 NTD strongly impaired S-mediated infection. Perhaps most notably, all individual mutations in the three serine residues in a small loop region (S371L/F, S373P, S375F), as well as the adjacent BA.2-specific T376A change severely impaired S-mediated infection.

Inefficient Processing and Virion Incorporation of Specific Spike Variants

To examine S expression, proteolytic processing and virions incorporation of the mutants, we performed comprehensive western blot analyses of HEK293T cells co-transfected with VSVΔG-eGFP and S expression constructs and the S-containing VSVpp in the culture supernatants. In agreement with the infectivity data, most individual amino acid changes, deletions or insertions had no significant impact on S expression and processing (Figure 3A). All 44 parental and mutant full-length S proteins were readily detected in the cellular extracts (Figure 3A). However,

mutations in S371L, S373P, S375F and T376A that impaired S infectivity (Figure 2) also reduced the efficiency of processing and/or incorporation into viral pseudoparticles (Figure 3A). The phenotypes of the S375F and T376A mutant were most striking and these S variants were hardly processed. Two BA.2 specific alterations in S (T19I and Δ24-26) that were less active in infection assays were associated with reduced levels of S protein on VSVpp (Figure 3A). Altogether, the levels of S2 protein expression and processing in cellular extracts relative to the parental Hu-1 S proteins correlated well with one another (Figure S2A) and with the efficiency of S-mediated infection (Figure 3B, left). Similar but less significant correlations were observed for the VSVpp infection and Spike levels in the culture supernatants (Figure 3B, right). T19I, Δ24-26, S375F and T376A reduced the levels of both S and S2 incorporated into VSVpp, while S371L/F mainly affected S2 levels in the particles. In comparison, mutations of Q493R, T547K, D796Y and N856K reduced VSVpp infection without exerting significant effects on S expression and processing in the cells although T547K and D796Y were associated with reduced levels of S2 in VSVpp (Figure 3). None of the mutations (H655Y, N679K and P681H) located near the S1/S2 cleavage site had significant effects on S processing (Figure 3). In addition, confocal microscopy showed that mutant S proteins showing enhanced (D614G, L981F) or impaired (T19I, S371L/F, S373P, S375F, T376A) activity all localized at the cell surface (Figure S2B) indicating that disruptive effects were not due to impaired trafficking or mislocalization. Altogether, our results revealed that changes of T19I, Δ24-26, T376A, S375F and Q954H reduce VSVpp infectivity by affecting S processing although they are not located in proximity to the S1/S2 furin cleavage site.

Functional relevance of serine mutations in an RBD loop region

It came as surprise that all individual mutations of S371, S373 and S375 that are found in the Wuhan Hu-1 strains and the Alpha, Beta, Gamma and Delta VOCs to 371L/F, 373P and 375F present in Omicron severely impaired S function. Analysis of available SARS-CoV-2 sequences revealed that the BA.1 and BA.2 S proteins usually contain combined changes of SxSxS to

FxPxF or LxPxF, respectively (Figure 4A). However, we identified a small subcluster within the BA.1 sequence showing reversions to serine residues. Phylogenetic analysis suggests that these occurred sequentially: from FxPxF to FxSxF to FxSxS to SxSxS (Figure 4A). The serine containing loop is located adjacent to the RBD and might affect its up and down state (Sztain et al., 2021) and stabilize RBD-RBD interactions (Wrobel et al., 2022) (Figure 4B). Altogether, the results suggested that the combination of S371-S373-S375 or 371F/L373P375F might be required for effective S function and processing. To address this experimentally, we generated the LPF (BA.1) and FPF (BA.2) triple mutants of the Hu-1 S protein and analysed their ability to mediate VSVpp infection. Both showed dramatically lower fusion activity (Figure 4C). In comparison, combined changes of S477N/T478K in the RBD and N764K/N856K/Q954H in S2 had only modest disruptive effects and alterations of N679K/P681H near the S2` processing site did not significantly change the infection efficiency of the Hu-1 S protein (Figure 4C). Intracellular localisation analyses showed that the LxPxF and FxPxF mutant S proteins were readily detectable at the cell surface, just like the parental Hu-1 S protein (Figure 4D). Thus, in agreement with the results on individual mutations (Figure S2B) the impaired activity and processing of the triple mutant S proteins is not due to altered trafficking or subcellular localization.

Effect of Mutations in Omicron Spike on ACE2 interaction and Cell-to-Cell Fusion

To examine the impact of specific mutations in the Omicron S protein on ACE2 interaction, we used a previously established *in vitro* S-ACE2 binding assay (Zech et al., 2021). Immobilized ACE2 is incubated with lysates of transfected HEK293T cells transfected with mutant S expression constructs. S protein retained after washing is detected by an αV5-Ms and quantified using a secondary HRP-conjugated anti-mouse Ab. The S371F, S373P, D614G, N856K and L981F mutations in the Hu-1 S had little if any effect on S binding to human ACE2 (Figure 5A). In comparison, individual substitutions of S375F and T376A and the triple mutations (SSS to

LPF or FPF) reduced the levels of S protein bound to ACE2 (Figure 5A). In line with published data (Tian et al., 2011), mutation of N501Y enhanced binding of the SARS-CoV-2 S protein to human ACE2 (Figure 5A).

Cell-to-cell fusion assays showed that co-expression of human ACE2 and the parental Hu-1 as well as the S373P, N501Y, D614G, N856K and L981F S proteins resulted in the formation of large syncytia (Figure 5B, 5C). In contrast, the S375F, T376A and triple LxPxF or FxPxF mutant S proteins did not lead to detectable fusion, while intermediate phenotypes were observed for the S371L and S371F Spikes (Figures 5B, 5C). In agreement with the VSVpp infection data, these results show that individual or combined mutations in S371, S373 and S375 or T376 disrupt the ability of the S protein to mediate membrane fusion.

Mutations of D614G and (to a stronger extent) L981F significantly increased syncytia formation (Figures 5B, 5C). L981 is located in the HR1 region of the S2 protein that interacts with HR2 to form a six-helix bundle to drive virus–host or cell-to-cell membrane fusion (Figure 5D). In agreement with the functional data, molecular modelling of HR1/HR2 interactions using reactive force field simulations predicted that mutation of L981F significantly enhances interactions between HR1 and HR2 (Figure 5D). Taken together, syncytia formation is promoted by D614G found in all VOCs and the Omicron-specific mutation L981F, but almost abrogated by S375F, T376A and the triple SSS to LPF or FPF changes.

Mutations in the Omicron S Affect Neutralization by Sera from Immunized Individuals

Recent studies have shown that the Omicron BA.1 and BA.2 Spikes show reduced sensitivity to neutralizing Abs induced upon infection and vaccination (Andrews et al., 2021; Cele et al., 2021; Hoffmann et al., 2021; Lu et al., 2021; Zhang et al., 2021). To determine the contribution of individual amino acid changes to immune evasion by Omicron, we compared the sensitivity of the four parental Hu-1, Delta, BA.1, BA.2 with 43 mutant S proteins, each harboring one Omicron-specific mutation, to neutralization by sera from five individuals who received a prime

boost vaccination with the mRNA-based BioNTech-Pfizer (BNT162b2) vaccine (Table S1). This vaccine has been approved in 141 countries (https://covid19.trackvaccines.org/vaccines/6/), is frequently used in Europe and the US, and induces efficient protection against most COVID-19 variants (Polack et al., 2020) but shows about 5- to 40-fold lower efficiency against Omicron (Cele et al., 2021; Collie et al., 2022; Iketani et al., 2022; Lu et al., 2021). Predictably, five randomly selected sera collected two weeks after the second dose of BNT neutralized BA.1 and BA.2 on average with substantially lower efficiency than the original Wuhan Hu-1 and Delta variants (Figure 6A; Table S1). A variety of shared as well as BA.1 or BA.2 specific amino acid changes reduced sensitivity to neutralization (examples shown in Figure 6A). It has been previously shown that the NTD contains important neutralizing epitopes (Chi et al., 2020) and that the mutations, deletions and insertions in this region are associated with significant structural changes (Zhang et al., 2022). Our analyses revealed that most individual mutations found in the NTD of BA.1 and BA.2 S proteins reduced neutralization sensitivity (Figure 6B). Deletion of residues 142-144 in BA.1 and G142D in BA.2 had the strongest effects (~9-fold reduction) followed by mutation of Y145D and 214EPE (both in BA.1) that conferred ~7-fold resistance. Amino acid changes in the RBD, such as G339D, S371L, S373P, K417N and N440K, as well as BA.2-specific alterations of S371F and R408S reduced sensitivity to neutralization by BNT/BNT sera, usually in the range of ~2- to 5-fold (Figure 6B). In comparison, five of the six mutations in the S2 region had little if any effect on neutralization. Only the N764K change reduced it on average about 2-fold. Altogether, 27 of the 43 mutations analyzed enhanced antibody-mediated neutralization resistance by >2-fold (Figure 6B). This further supports that a large number of substitutions in the Omicron Spike cooperates to allow efficient viral evasion of humoral immune responses.

In the final set of experiment, we examined the impact of specific mutations in the Omicron S protein on neutralization sensitivity to the FDA-approved therapeutic monoclonal antibodies REGN10987 (marketed as imdevimab), LY-CoV555 (marketed as bamlanivimab) and REGN10933 (marketed as casivirimab). The BA.1 VOC was not inhibited by imdevimab and the N440K or G446S mutations in the Hu-1 S were sufficient to confer full resistance (Figure 7). In contrast, BA.2 S remained susceptible to imdevimab and changes of E484A, Q493R and G496S had little effect. In comparison, both BA.1 and BA.2 were fully resistant to bamlanivimab and substitutions of E484A or Q493R were sufficient to confer resistance (Figure 7). These results agree with those of two recent studies that also examined the impact of individual amino acid changes found in the BA.1 and BA.2 spikes on neutralization by a panel of monoclonal antibodies (Iketani et al., 2022; Liu et al., 2022). Finally, casivirimab showed no appreciable activity against BA.1 but neutralized BA.2 and all mutant S proteins analyzed, albeit with lower efficacy compared to the original Hu-1 S (Figure 7). Altogether, our results show that a strikingly high number of amino acid changes in the NTD and RBD regions of the Omicron S proteins contribute to evasion from neutralizing antibodies. The impact of individual mutations on susceptibility to neutralization varies strongly between sera obtained from individuals who received the BNT/BNT vaccine.

DISCUSSION

The Omicron VOC has outcompeted the previously dominating Delta VOC in an amazingly short time. It is generally accepted that the high number of changes in Omicron S are the main reason for effective spread of this VOC and confer increased transmission efficiency and escape from neutralizing antibodies. Here, we systematically analyzed the functional impact of all individual amino acid changes, deletions and insertions that are characteristic for the Omicron BA.1 and BA.2 VOCs. In total, we examined 48 mutant Spike constructs containing amino acid changes distinguishing BA.1 and BA.2 Omicron VOCs from the original Hu-1 Wuhan strain. We identified several changes that strongly impair Spike-mediated infection and proteolytic processing. In addition, we demonstrate that BA.1 or BA.2 specific mutations in the NTD as well as shared alterations in the RBD significantly reduce the susceptibility of Spike containing VSVpp to neutralization by sera from BNT/BNT vaccinated individuals and therapeutic antibodies.

One striking finding was that individual mutations of S371F/L, S375F, T376A and (to a lesser extent) S373P in the receptor binding domain strongly impair Spike-containing pseudoparticle infectivity and Spike processing. S375F had the most drastic effect and almost fully disrupted Spike function and processing. This agrees with a recent preprint (Yamasoba et al., 2022) and is of particular interest because it has recently been reported that the S371L and S371F mutations in BA.1 and BA2, respectively, have major effects on neutralization by different RBD classes (Liu et al., 2021; Iketani et al., 2022). However, our results show that although these mutations significantly reduce S-mediated infection (Figure 2) they have only modest effects on neutralization by BNT/BNT sera (Figure 6). Notably, all these residues are part of a loop that may affect the open and closed conformation of the RBD. Recent structural analyses show that mutations of S371L, S373P and S375F promote interprotomer interactions between the “down” RBDs (Gobeil et al., 2022). Specifically, it has been proposed that the S373P substitution induces

conformational changes of the loop resulting in closer packing of the RBD-RBD interface via interactions of S373P and S375F with the N501Y and Y505H substitutions in the adjacent RBD (Gobeil et al., 2022). Our functional analyses show that mutations of S371L/F and T376A severely affect Spike function, while changes of N501Y and Y505H had no disruptive effects on S-mediated infection. Both individual and combined mutations in the three serine residues (S371, S373 and S375) severely impaired the ability of the Hu-1 Spike protein to mediate virus-cell and cell-cell fusion. While further studies are necessary, it is tempting to speculate that, in the absence of additional alterations, changes of S371L, S373P, S375F and perhaps T376A might stabilize the inactive closed conformation of the Spike protein. The severe disruptive effects also raise questions whether they are associated with a selection advantage. Our identification of a subcluster of BA.1 isolates that sequentially reverts to the original sequence (FxPxF to FxSxF to FxSxS to SxSxS; Figure 4A) indicates that this may not be the case and it will be of significant interest to closely monitor the frequency of Omicron variants containing alterations in the serine containing loop region.

A variety of mutations in the S1 subunit (ΔH69/V70, T95I, ΔY144, K417N, T478K, N501Y, D614G, H655Y and P681H) of BA.1 and/or BA.2 Omicron S proteins have previously been observed in other VOCs (Golcuk et al., 2021). As previously suggested (Mannar et al., 2022), we found that deletion of ΔH69/V70 increased S-mediated infectivity (Figure 2). Our analyses also confirmed (Lam et al., 2021) that mutation of N501Y in the RBM of the Omicron Spike increases the binding affinity to ACE2 (Figure 5A). It has been proposed that mutations of H655Y, N679K and P681H may increase furin-mediated S1/S2 cleavage and enhance pseudoparticle infectivity (Aggarwal et al., 2021; Cameroni et al., 2021; VanBlargan et al., 2022). We found that none of these three changes significantly enhanced S-mediated VSVpp infection (Figure 2) and only H655Y clearly enhanced S processing (Figure 3). Mutations of K417N, Q493R, Q498R and N501Y are identical or similar to changes emerging during SARS-

CoV-2 adaptation to experimentally infected mice (Huang et al., 2021; Sun et al., 2021), and were proposed to stabilize the RBD and ACE2 interaction (Meng et al., 2022) or to contribute to the ability of Omicron to infect mouse cells (Hoffmann et al., 2021). However, individual changes had no significant effect on VSVpp infectivity or processing but reduced susceptibility to BNT/BNT neutralization. Similarly, based on cryo-EM analyses it has been suggested that alterations of Q493R, G496S and Q498R in the RBD of the Omicron S form may allow the formation of stronger interactions with ACE2 that compensate for a disruptive effect of K417N (Mannar et al., 2022) but none of these four mutations individually significantly affected S-mediated infection (Figure 2).

Predictably, many shared mutations in the RBD domain of BA.1 and BA.2 S proteins reduced the sensitivity of VSVpp to neutralization by sera from BNT/BNT vaccinated individuals (Figure 6A). In addition, we also found that mutations of N440K or G446S conferred resistance to imdevimab and changes of E484A or Q493R to bamlanivimab, respectively. This was expected since these mutations are located within the epitopes bound by these antibodies (Figure 6B, 6C). Our results add to the evidence (Iketani et al., 2022; Liu et al., 2022) that single amino acid changes may confer full resistance to neutralizing antibodies. In comparison, mutation of E484A that has also been observed in other SARS-CoV-2 VOCs and was suggested to be associated with immune-escape (Rath et al., 2022) had only marginal effects on neutralization sensitivity. Unexpectedly, most lineage-specific changes in the NTD, such as A27S, T95I, Δ142-144, G142D, INS214EPE, L212I and V213G, were at least as effective in reducing S sensitivity to neutralization by sera from BNT/BNT vaccinated individuals as changes in the RBD (Figure 6A). This supports a key role of the NTD as target for neutralizing antibodies in sera from vaccinated individuals.

Three mutations (Q954H, N969K and L981F) are located in the HR1 region of the S2 subunit of the S protein (Figure 1D). It has been initially proposed that these changes may promote 6-

helix bundle formation and subsequent fusion (Sarkar et al., 2021) but more recent evidence suggests that they may attenuate rather than enhance S-mediated fusion efficiency (Suzuki et al., 2022). In agreement with the latter, changes of Q954H and N969K clearly reduced S-mediated VSVpp infection (Figure 2). In contrast, substitution of L981F enhanced Spike-mediated VSVpp infection and (more strongly) cell-to-cell fusion (Figure 5B). Reactive force simulations suggest that the L981F mutation enhances interactions between the HR1 and HR2 regions that drive fusion. Notably, recent data showed that the three mutations in the HR1 region of the Omicron S do not alter the global architecture of the post-fusion six-helix bundle (Yang et al., 2022) and peptide-based pan-CoV fusion inhibitors derived from the HR region maintain high potency against the SARS-CoV-2 Omicron VOC (Xia et al., 2022).

The molecular mechanisms of several mutations in the Omicron S protein remain to be fully elucidated. For example, BA.2-specific changes of T19I and Δ24-26 in the NTD severely reduced S-mediated infection and processing although they do not affect known functional domains. It has been suggested that a shared mutation of N764K and a BA.2-specific substitution of N856K generate potential cleavage sites for SKI-1/S1P protease and might impede the exposition of the fusion peptide for membrane fusion (Maaroufi, 2022). We found that N764K is indeed associated with increased infectivity and increased levels of processed Spike in VSVpp. In comparison, N856K clearly reduced S-mediated infection despite normal processing.

Limitations of the study

In the present study, we used pseudotyped viral particles instead of replication-competent recombinant SARS-CoV-2 variants, which serves as a proxy to assess infectivity, fusion activity and incorporation. In addition, the impact of many changes might be context-dependent and this might explain why some individual changes had disruptive effects on Hu-1 S function although they are found in Omicron S proteins. It is difficult to predict which of the numerous mutations in the Omicron S might compensate for disruptive mutations. For example, we found that the

BA.1 S was less effective in mediating infection than the BA.2 S protein (Figure 2). This agrees, with accumulating evidence that the BA.2 VOC might be more infectious and more virulent than the BA.1 VOC (Suzuki et al., 2022). In addition, we analysed only a limited number of sera from individuals who received a single vaccine regimen (BNT/BNT) and just a few therapeutic antibodies. While further studies are required to fully understand the full consequences of all the complex changes in the Omicron Spike on viral infectivity, tropism, transmission and pathogenesis our results provide first important insights into the functional impact of mutations characteristic for the Omicron VOC Spike that currently dominates the pandemic.

ACKNOWLEDGEMENTS

We thank Kerstin Regensburger, Regina Burger, Jana-Romana Fischer, Birgit Ott, Martha Meyer, Nicola Schrott and Daniela Krnavek for technical assistance and Dorota Kmiec for critical reading of our manuscript. The ACE2 expression vector and SARS-CoV-2 S-HA plasmid were kindly provided by Shinji Makino and Stefan Pöhlmann. C.P. and S.N. are part of the International Graduate school for Molecular Medicine (IGradU). This study was supported by DFG grants to F.K. (CRC 1279, SPP 1923), K.M.J.S. (CRC 1279, SPP 1923, SP 1600/6-1) and T.J. (CRC 1279). F.K., and K.M.J.S. were supported by the BMBF (Restrict SARS-CoV-2 and IMMUNOMOD).

CONTRIBUTIONS

C.P. and F.Z. performed most experiments with support by S.N. F.Z., K.M.J.S., and F.K. conceived the study and planned experiments. C.J. and T.J. performed molecular modelling and dynamics simulations. F.K. wrote the initial draft of the manuscript. All authors reviewed and approved the manuscript.

DECLARATION OF INTERESTS

All authors declare no competing interests

MAIN FIGURE LEGENDS

Figure 1. Features of Omicron BA.1 and BA.2 VOCs.

(**A**) Radial phylogenetic tree of representative SARS-CoV-2 strains (n= 2863 genomes, sampled between Dec 2019 and Mar 2022) scaled according to their divergence compared to the Wuhan Hu-1 sequence. Retrieved from Nextstrain on April 7th 2022 (https://nextstrain.org/ncov/gisaid/global?m=div) and modified. Colour coding according to VOCs as indicated.

(**B**) Frequencies of SARS-CoV-2 Delta, BA.1 and BA.2 sequences in data from GenBank from September 1st 2021 to 7th of April 2022. Scaled to 100%. Retrieved and modified from Nextstrain on April 7th 2022. Orange, Delta VOC. Purple, BA.1. Green, BA.1.

(**C**) Overview on the SARS-CoV-2 spike structure (downloaded from PDB: 7KNB) and localization of amino acid changes that are shared between BA.1 and BA.2 or specific for BA.1 or BA.2 as indicated. S1 (orange), S2 (blue) ACE2 (grey), mutations (red), BA.1 specific deletions (blue), BA.2 specific deletions (yellow).

(**D**) Schematic depiction of the SARS-CoV-2 spike, its domains and amino acid alterations in Omicron BA.1 (dark green) and BA.2 (light green) VOC compared to the Wuhan Hu-1 sequence. S1 subunit: N-terminal domain, NTD (purple) and receptor binding domain, RBD (orange). Receptor binding motif, RBM (dark orange). S2 subunit: fusion peptide, FP (blue), heptad repeat 1, HR1 (dark blue) central helix, CH, connector domain, CD, heptad repeat 2, HR2, and transmembrane domain, TM (blue).

Figure 2. Impact of mutations in Omicron on Spike-mediated infection.

(**A**) Automatic quantification of infection events of CaCo-2 cells transduced with VSVΔG-GFP pseudotyped with SARS-CoV-2 Hu-1 (grey), Delta (turquise), BA.1 (dark green), BA.2 (light green) or indicated mutant S proteins. The localisation of each mutation in S is indicated by colour. S1: NTD (purple), RBD (orange), RBM (dark orange), others (light orange), S2: HR1 (dark blue) others (light blue). Bars represent the mean of three independent experiments (±SEM). Statistical significance was tested by one-way ANOVA. *P < 0.05; **P < 0.01; ***P < 0.001.

(**B**) Infection kinetics of CaCo-2 cells infected by VSVpp containing the indicated mutant S proteins. Infected cells were automatically quantified over a period of 22 h.

See also Figure S1.

Figure 3. Expression and processing of Spike proteins containing mutations present in the Omicron BA.1 and BA.2 VOCs.

(**A**) The upper panels show exemplary immunoblots of whole cells lysates (WCLs) and VSVpp containing supernatants of HEK293T cells transfected with vectors expressing the Hu-1 or mutant SARS-CoV-2 S proteins and VSVΔG-GFP constructs. Blots were stained with anti-V5 (Spike), anti-ß-actin and anti-VSV-M protein. Lower panels: expression levels of uncleaved, full-length Spike protein (S, gray bars) and the S2 subunit (bars coloured according to the corresponding domains as shown in Figure 1D) were quantified. The results show mean values (±SEM) obtained from three independent experiments.

(**B**) Correlation of the S2 expression/incorporation and S/S2 processing of the parental S Hu-1 or indicated mutant S proteins in cells and supernatants with the corresponding pseudotype infection rates. Coefficient of determination (R^2-values) and two tailed P values are provided.

See also Figure S2.

Figure 4. Evolution and functional relevance of S371L/F, S373P and S375F changes in the Spike protein.

(A) Phylogenetic tree of Delta, Omicron BA.1 and BA.2 strains. Amino acids at position 371, 373 and 375 are indicated; all other SARS-CoV-2 variants almost invariantly contain three serines at these positions. Colour coding as indicated according to VOC. Retrieved and modified from Nextstrain on April 7th 2022.

(**B**) Close-up view of the region encompassing the mutations S371L, S373P and S375F and the surrounding region. Downloaded from PDB: 7KNB, 7TGW or 7WKA as indicated.

(**C**) Automatic quantification of infection events of CaCo-2 cells transduced with VSVΔG-GFP pseudotyped with SARS-CoV-2 Hu-1 or indicated combined mutations. Bars represent the mean of three independent experiments (±SEM). Statistical significance was tested by one-way ANOVA. *P < 0.05; **P < 0.01; ***P < 0.001.

(**D**) Immunofluorescence images of HEK293T cells expressing the parental S Hu-1, the BA.1 specific S37xLPF or the BA.2 specific S37xFPF mutations. Scale bar, 10 µm.

Figure 5. ACE2 interaction of Spike variants

(**A**) Binding of the indicated Hu-1 and mutant S proteins to ACE2 binding using whole cell lysates of transfected HEK293T. Bars represent the mean of three independent experiments (±SEM). Statistical significance was tested by one-way ANOVA. *P < 0.05; **P < 0.001.

(**B**) Representative fluorescence microscopy images of HEK293T cells expressing parental Hu-1 or indicated mutant S proteins, Human ACE2 and GFP (green). Scale bar, 125 µm.

(**C**) Automatic quantification of syncytia formation of HEK293T cells expressing parental Hu-1 or indicated mutant S proteins and Human ACE2. Bars represent the mean of three independent experiments (±SEM). Statistical significance was tested by two-tailed Student's t-test with Welch's correction. *P < 0.05; **P < 0.01; ***P < 0.001.

(**D**) Overview on the SARS-CoV-2 post-fusion spike structure (downloaded from PDB: 6M3W) and comparative ReaxFF simulation of the mutation L981F.

Figure 6. Impact of mutations in the Omicron Spike on serum neutralization.

(**A**) Neutralization of VSVpp carrying the indicated wildtype and mutant S proteins by sera obtained from five BNT/BNT vaccinated individuals compared to the untreated control (set to one). Shown are mean values obtained for the five sera, each tested in three independent experiments.

(**B**) Changes in $TCID_{50}$ values obtained for neutralization of the indicated mutant S proteins by sera from five vaccinated individuals relative to those obtained for the Hu-1 S. Solid red bars indicate average values (±SEM) for the five sera and open black squares the average infectivity of the respective S containing VSVpp shown in Figure 2A.

See also Figure Table S1.

Figure 7. Impact of mutations in the Omicron Spike on neutralization by therapeutic Abs.

Close-up view of neutralising antibodies binding the SARS-CoV-2 Spike (PDB: 6XDG or 7L3N as indicated) and automated quantification of GFP fluorescence of Caco-2 cells infected with VSVΔG-GFP pseudotyped with the indicated S variants. VSVpp were pre-treated (30 min, 37 °C) with the indicated amounts of Imdevimab, Bamlanivimab or Casivirimab. Lines represent the mean of three independent experiments.

STAR METHODS

RESOURCE AVAILABILITY

Lead contact

Further information and requests for resources and reagents should be directed to and will be fulfilled by the Lead Contact, Frank Kirchhoff (frank.kirchhoff@uni-ulm.de)

Materials Availability

All unique reagents generated in this study are listed in the Key Resources Table and available from the Lead Contact.

Data and code availability

This study did not generate or analyse datasets or codes.

METHOD DETAILS

Cell Culture. All cells were cultured at 37 °C and 5% CO_2 in a humified atmosphere. HEK293T (human embryonic kidney) cells (ATCC: #CRL3216) were maintained in Dulbecco's Modified Eagle Medium supplemented with 10% (v/v) heat-inactivated fetal calf serum, 2 mM L-glutamine, 100 µg/ml streptomycin and 100 U/ml penicillin. Caco-2 (human epithelial colorectal adenocarcinoma) cells were cultivated in DMEM containing 10% FCS, 2mM glutamine, 100 µg/ml streptomycin and 100 U/ml penicillin, 1mM NEAA supplement. Mouse I1-Hybridoma cells (ATCC: #CRL2700) were cultured in Roswell Park Memorial Institute (RPMI) 1640 medium supplemented with 10% (v/v) heat-inactivated fetal calf serum, 2 mM L-glutamine, 100 µg/ml streptomycin and 100 U/ml penicillin.

Expression Constructs. pCG_SARS-CoV-2-Spike-IRES_eGFP encoding the spike protein of SARS-CoV-2 isolate Wuhan-Hu-1(NCBI reference Sequence YP_009724390.1), pCG_SARS-CoV-2-S (1.617), pCG1_SARS-2-S (B.1.1.529) and pCG1_SARS-2-SΔ18 (BA.2) were kindly provided by Stefan Pöhlmann (DPZ Göppingen, Germany). pCG_SARS-CoV-2-Spike C-V5-IRES_eGFP was PCR amplified and subcloned into a pCG-IRES_eGFP expression construct using the restriction enzymes XbaI+MluI. The SARS-CoV-2 S mutant plasmids were generated using Q5 Site-Directed Mutagenesis Kit (NEB #E0554). ACE2 was synthezised by Twist bioscience, PCR amplified, and subcloned into a pCG-IRES_eGFP expression construct using the restriction enzymes XbaI+MluI. All constructs were verified by sequence analysis using a commercial sequencing service (Eurofins Genomics).

Molecular dynamics simulation. Initial atomic positions of ACE2-bound to SARS-CoV-2 spike (7KNB, https://www.rcsb.org/structure/7KNB) respectably the post-fusion structure of SARS-CoV-2 spike glycoprotein (PDB id 6M3W https://www.rcsb.org/structure/6m3w) were obtained from the Protein Data Bank (Bernstein et al., 1977). Equilibrations (300 K for 0.5 ns) were performed by ReaxFF (reactive molecular dynamic) simulations (Adri C. T. van Duin et al., 2001) within the Amsterdam Modelling Suite 2020 (http://www.scm.com). Based on the equilibrated structures, amino acids from the Wuhan-1 spike protein were replaced with the respective amino acids from Omicron BA.1 and BA.2 spike protein. These modified structures were additionally equilibrated (300 K for 0.5 ns) ReaxFF (reactive molecular dynamic) within an NVT while coupling the system to a Berendsen heat bath (T = 300 K with a coupling constant of 100 fs). The interaction energies were obtained by averaging over the last 0.1 ns of these simulations. The Visual Molecular Dynamics program (VMD 1.9.3) (Humphrey et al., 1996) was used for all visualizations.

Pseudoparticle Production. To produce pseudotyped VSV(GFP)ΔG particles, HEK293T cells were transfected with Spike-expressing vectors using polyethyleneimine (PEI 1 mg/ml in H_2O). Twenty-four hours post-transfection, the cells were infected with VSVΔG(GFP)*VSV-G at a MOI of 3. The inoculum was removed 1hour post-infection. Pseudotyped VSVΔG-GFP particles were harvested 16 h post-infection. Remaining cell debris were removed by centrifugation (500 × g for 5 min). Residual particles carrying VSV-G were blocked by adding 10% (v/v) of I1-Hybridoma supernatant (I1, mouse hybridoma supernatant from CRL-2700; ATCC) to the cell culture supernatant.

Infection Assay. Caco-2 cells were infected with 100 µl of VSVΔG-GFP pseudo particles in 96 well format. GFP-positive cells were automatically counted using a Cytation 3 microplate reader (BioTek Instruments).

Pseudoparticle inhibition. 50 µl of VSVΔG-GFP pseudo particles were preincubated for 30 min at RT with the indicated amounts of monoclonal antibodies (Bamlanivimab, Imdevimab, Casivirimab) or sera from fully BNT162b2 vaccinated individuals and transduced on CaCo-2 cells in 96 well format. 24 hours after infection, GFP-positive cells were automatically counted by a Cytation 3 microplate reader (BioTek Instruments).

Sera from vaccinated individuals. Blood samples of fully BNT162b2 vaccinated individuals were obtained after the participants information and written consent. Samples were collected 13−30 days after the second vaccination using S-Monovette Serum Gel tubes (Sarstedt). Before

use, the serum was heat-treated at 56 °C for 30 min. Ethics approval was provided by the Ethic Committee of Ulm University (vote 99/21– FSt/Sta).

Whole-cell and cell-free lysates. To prepare whole-cell lysates, cells were collected and washed in phosphate-buffered Saline (PBS), pelleted and lysed in transmembrane lysis buffer, containing protease inhibitor (1:500). After 5 min of incubation on ice, supernatants were cleared by centrifugation (4 °C, 20 min, 20,817 × g). To prepare WB lysates of viral particles, the supernatants were layered on a cushion of 20% sucrose and centrifuged (4 °C, 90 min, 20,817 × g). The virus pellet was lysed in transmembrane lysis buffer, mixed with 4x Protein Sample Loading Buffer (LI-COR) containing 10% β-mercaptoethanol (Sigma Aldrich) and denaturized at 95 °C for 10 min.

SDS-PAGE and immunoblotting. SDS-PAGE and immunoblotting was performed as previously described (Zech et al. 2021). In brief, whole cell lysates were mixed with 4x Protein Sample Loading Buffer (LI-COR) containing 10% β-mercaptoethanol (Sigma Aldrich), heated at 95 °C for 20 min, separated on NuPAGE 4-12% Bis-Tris Gels (Invitrogen) for 90 min at 120 V and blotted at constant 30 V for 30 min onto Immobilon-FL PVDF membrane. After the transfer, the membrane was blocked in 1% Casein in PBS. Proteins were stained using primary antibodies directed against rabbit anti-V5 (Cell Signaling #13202; 1:1000), VSV-M (Absolute Antibody, 23H12, #Ab01404-2.0; 1:2000), actin (Anti-beta Actin antibody Abcam, ab8227, 1:5000,) and Infrared Dye labeled secondary antibodies (LI-COR IRDye) IRDye 800CW Goat anti-Mouse #926-32210, IRDye 680CW Goat anti-Rabbit (#925-68071), all 1:20,000. Proteins were detected using a LI-COR Odyssey scanner and band intensities were quantified using LI-COR Image Studio version 5.

ACE2 interaction assay. HEK293T cells expressing Spike were collected 48 h after the transfection, washed with phosphate-buffered saline (PBS), lysed in a non-denaturizing lysis buffer. Interaction between Spike protein and ACE2 was assessed through a Spike-ACE2 binding assay kit (COVID-19 Spike-ACE2 binding assay II, Ray Bio). Briefly, 10 µl of WCLs were diluted 1:5 in 1x assay diluent buffer (RayBio), added to ACE2 coated wells (RayBio) and incubated for 2 h with shaking. After washing extensively with the provided wash buffer (RayBio, #EL-ITEMB), the wells were incubated 1 h with 100 µl anti-V5(MS) (1:1,000, Cell Signalling, #80076), washed and incubated for 1 h with 100 µl anti-MS-HRP (1:1,000, RayBio). After washing, the samples were incubated with 50 µl of TMB Substrate Solution (RayBio, #EL-

TMB) for 30 min. The reaction was stopped by the addition of 50 µl Stop Solution (RayBio, #ELSTOP) and absorbance was measured at 450 nm with a baseline correction at 650 nm.

Immunofluorescence. HEK293T cells were plated in 12-well tissue culture dishes on 13-mm round borosilicate cover slips pre-coated with poly-L-lysine. 24 hours after, the cells were transfected with expression constructs for Spike protein using polyethyleneimine (PEI 1 mg/ml in H_2O). 24 hours after transfection, cells were washed with cold PBS and fixed in 4% paraformaldehyde solution (PFA) for 20 min at RT, permeabilized and blocked in PBS containing 0.5% Triton X-100 and 5% FCS for 30 min at RT. Thereafter, samples were washed with PBS and incubated for 2 h at 4°C with primary antibody (anti-V5(MS) (1:1,000, Cell Signalling, #80076)) diluted in PBS. The samples were washed with PBS/0.1% Tween 20 and incubated in the dark for 2 h at 4°C with the secondary antibody (Alexa Fluor-647-conjugated anti-mouse antibody, 1:1000, Thermo Fisher Scientific) and 500 ng/ml DAPI. After washing with PBS-T and water, cover slips were mounted on microscopy slides. Images were acquired using a Zeiss LSM800 confocal laser scanning microscope with ZEN imaging software (Zeiss).

Quantification of syncytia formation. To detect formation of syncytia, HEK293T cells were co-transfected with ACE2 and Spike expressing vectors using polyethyleneimine (PEI 1 mg/ml in H_2O). Twenty-four hours post-transfection, fluorescence microscopy images were acquired using the Cytation 3 microplate reader (BioTek Instruments) and the GFP area was quantified using ImageJ.

Statistical analysis. Statistical analyses were performed using GraphPad PRISM 9.2 (GraphPad Software). P-values were determined using two-tailed Student's t-test with Welch's correction or One-Way ANOVA with multiple comparison against the Wuhan-Hu-1 values. Unless otherwise stated, data are shown as the mean of at least three independent experiments ± SEM. Significant differences are indicated as *p <0.05; **p < 0.01; ***p < 0.001.

619 **Key resources table**

REAGENT or RESOURCE	SOURCE	IDENTIFIER
Antibodies		
Mouse monoclonal anti-V5 Spike	Cell Signaling Technology	Cat#80076S
Alexa Fluor 647 goat anti-mouse IgG (H+L)	Thermo Fisher	Cat#A-11004; RRID: AB_2534072
Rabbit monoclonal anti-V5 Spike	Cell Signaling Technology	Cat#13202S; RRID: AB_2687461
Mouse monoclonal anti-VSV-M (23H12)	Absolute Antibody	Cat#Ab01404-2.0
Rabbit polyclonal anti-beta Actin	Abcam	Cat#ab8227; RRID: AB_2305186
IRDye 800CW Goat anti-Mouse IgG (H + L)	LI-COR	Cat#926-32210; RRID: AB_621842
IRDye 680CW Goat anti-Rabbit IgG (H + L)	LI-COR	Cat#925-68071; RRID: AB_2721181
Bamlanivimab	Lilly Pharma	LY-CoV555 700 mg; Lot#D336907A
Imdevimab	Roche	REGN10897 1332 mg; Lot#N7534
Casivirimab	Roche	REGN10933 1332 mg; Lot#N7533
Bacterial and virus strains		
NEB® 5-alpha Competent E. coli (High Efficiency)	New England BioLabs	Cat#C2987H
XL2-Blue MRF' TM Ultracompetent cells	Agilent Technologies	Cat#200151
VSVΔG(GFP)*VSV-G	Kindly provided by Prof. Karl-Klaus Conzelmann, Institute of Virology, LMU Munich, Germany	N/A
Biological samples		
Human sera	This study	N/A
Chemicals, peptides, and recombinant proteins		
DAPI	Sigma-Aldrich	D9542-1MG; CAS: 28718-90-3
L-Glutamine	PANBiotech	Cat#P04-80100
Penicillin-Streptomycin	PANBiotech	Cat#P06-07100
Complete ULTRA inhibitor cocktail tablet	Roche	Cat#05892791001

2-Mercaptoethanol	Sigma-Aldrich	Cat#M6250-100ML
Polyethyleneimine (PEI)	Sigma-Aldrich	Cat#408727-100ML
4 % Paraformaldehyde (PFA)	ChemCruz	Cat#sc-281692
4X Protein Sample Loading Buffer	LI-COR	Cat#928-40004
Glycerol	Sigma-Aldrich	Cat#G5516-500ML
Mowiol 4-88	ROTH	Cat#0713.1
Tween 20	Sigma-Aldrich	Cat#P7949-500ML
Tris-Cl	Sigma-Aldrich	Cat#T5941-500G
DABCO (1,4-diazabicyclo-[2,2,2]-octane)	ROTH	Cat#0718.1
HEPES	Sigma-Aldrich	Cat#H3375-250G
NaCl	Sigma-Aldrich	Cat#106404
Triton X-100	Sigma-Aldrich	Cat#T9284-100ML
Ethylenediaminetetraacetic acid (EDTA)	Sigma-Aldrich	Cat#EDS-100G
Trypsin/EDTA 0.05 % / 0.02 %	PANBiotech	Cat#P10-023100
Dulbecco's Phosphate Buffered Saline (PBS)	Thermo Fisher	Cat#14190094
Poly-L-Lysine	Sigma-Aldrich	Cat#P6282-5MG
Fetal Bovine Serum	Thermo Fisher	Cat#10270106
0.5 % Trypsin-EDTA	Thermo Fisher	Cat#15400054
Blocker Casein in PBS	Thermo Fisher	Cat#37528
Critical commercial assays		
Q5 Site-Directed Mutagenesis Kit	New England BioLabs	Cat#E0554
COVID-19 Spike-ACE2 Binding Assay Kit	RayBiotech	Cat#QHD43416
Deposited data		
Raw and analyzed data	This study	N/A
Experimental models: Cell lines		
Human: HEK293T cells	ATCC	CRL-3216; RRID: CVCL_0063
Human: CaCo-2 cells	ATCC	HTB-37; RRID: CVCL_0025
Mouse: I1 Hybridoma cells	ATCC	CRL-2700; RRID: CVCL_G654
Experimental models: Organisms/strains		

Oligonucleotides		
Primers for designing the Omicron Spike mutants, see Table Primer	This study	N/A
Recombinant DNA		
Plasmid: pCG_SARS-CoV-2-Spike-IRES_eGFP	This study	N/A
Plasmid: SARS-CoV-2 Spike Protein (YP_009724390.1)	R&D	Cat#RDC3074
Plasmid: pCG_SARS-CoV-2-S (1.617)	Stefan Pöhlmann, DPZ, Göttingen, Germany	N/A
Plasmid: pCG1_SARS-2-S (B.1.1.529)	Stefan Pöhlmann, DPZ, Göttingen, Germany	N/A
Plasmid: pCG1_SARS-2-SΔ18 (BA.2)	Stefan Pöhlmann, DPZ, Göttingen, Germany	N/A
Software and algorithms		
GraphPad Prism Version 9.2	GraphPad Software, Inc.	https://www.graphpad.com RRID: SCR_002798
LI-COR Image Studio Version 5.2	LI-COR	www.licor.com/ RRID: SCR_015795
CorelDRAW 2021 (64-Bit)	Corel Corporation	www.coreldraw.com/ RRID: SCR_014235
BioTek Gen5 3.04	Agilent Technologies	www.biotek.com
Fiji 1.53	National Institutes of Health (NIH)	imagej.nih.gov/ij/ RRID: SCR_003070
Amsterdam Modeling Suite 2020	Software for Chemistry & Materials BV	www.scm.com
Visual Molecular Dynamics 1.9.3	NIH Center for Macromolecular Modeling & Bioinformatics	www.ks.uiuc.edu/
ZEN (black edition)	Carl Zeiss Microscopy GmbH	www.micro-shop.zeiss.com RRID: SCR_013672
Other		
Dulbecco's Modified Eagle Medium	Thermo Fisher	Cat#41965039
Roswell Park Memorial Institute Medium 1640	Thermo Fisher	Cat#21875034

MEM Non-essential amino acids	Thermo Fisher	Cat#11140035
Opti-MEM Reduced Serum Media	Thermo Fisher	Cat#31985047
Saccharose	Sigma-Aldrich	Cat#S0389-500G
NuPAGE 4-12% Bis-Tris Gels	Invitrogen	Cat#NP0323BOX
Immobilon-FL PVDF membrane	Sigma-Aldrich	Cat#IPFL00010
Borosilicate Cover Slips, 13 mm	VWR	Cat#6310150
XbaI restriction enzyme	New England BioLabs	Cat#R0145
MluI restriction enzyme	New England BioLabs	Cat#R0198

620

621

622 **REFERENCES**

623 Adri C. T. van Duin, Siddharth Dasgupta, Francois Lorant, and William A. Goddard (2001).
624 ReaxFF: A Reactive Force Field for Hydrocarbons. J. Phys. Chem. A, 105, 9396–9409.

625 Aggarwal, A., Stella, A.O., Walker, G., Akerman, A., Milogiannakis, V., Brilot, F., Amatayakul-
626 Chantler, S., Roth, N., Coppola, G., Schofield, P., et al. (2021). SARS-CoV-2 Omicron: evasion
627 of potent humoral responses and resistance to clinical immunotherapeutics relative to viral
628 variants of concern. medRxiv, doi: https://doi.org/10.1101/2021.12.14.21267772

629 Altarawneh, H.N., Chemaitelly, H., Hasan, M.R., Ayoub, H.H., Qassim, S., AlMukdad, S.,
630 Coyle, P., Yassine, H.M., Al-Khatib, H.A., Benslimane, F.M., et al. (2022). Protection against
631 the Omicron Variant from Previous SARS-CoV-2 Infection. New England Journal of Medicine
632 *386*, 1288–1290. https://doi.org/10.1056/NEJMc2200133.

633 Andrews, N., Stowe, J., Kirsebom, F., Toffa, S., Rickeard, T., Gallagher, E., Gower, C., Kall,
634 M., Groves, N., O'Connell, A.-M., et al. (2021). Effectiveness of COVID-19 vaccines against
635 the Omicron (B.1.1.529) variant of concern. medRxiv, doi: https://doi.org/10.1101/2021.12.14.
636 21267615.

637 Bernstein, F.C., Koetzle, T.F., Williams, G.J., Meyer, E.F., Brice, M.D., Rodgers, J.R., Kennard,
638 O., Shimanouchi, T., and Tasumi, M. (1977). The Protein Data Bank: a computer-based archival
639 file for macromolecular structures. Journal of Molecular Biology *112*, 535–542.
640 https://doi.org/10.1016/s0022-2836(77)80200-3.

641 Cameroni, E., Saliba, C., Bowen, J.E., Rosen, L.E., Culap, K., Pinto, D., Marco, A.D., Zepeda,
642 S.K., Iulio, J. di, Zatta, F., et al. (2021). Broadly neutralizing antibodies overcome SARS-CoV-
643 2 Omicron antigenic shift. Nature *602*, 664–670.

644 Cele, S., Jackson, L., Khoury, D.S., Khan, K., Moyo-Gwete, T., Tegally, H., San, J.E., Cromer,
645 D., Scheepers, C., Amoako, D.G., et al. (2021). Omicron extensively but incompletely escapes
646 Pfizer BNT162b2 neutralization. Nature *602*, 654-656.

647 Chen, T.-W., Wardill, T.J., Sun, Y., Pulver, S.R., Renninger, S.L., Baohan, A., Schreiter, E.R.,
648 Kerr, R.A., Orger, M.B., Jayaraman, V., et al. (2013). Ultrasensitive fluorescent proteins for
649 imaging neuronal activity. Nature *499*, 295–300.

650 Chi, X., Yan, R., Zhang, J., Zhang, G., Zhang, Y., Hao, M., Zhang, Z., Fan, P., Dong, Y., Yang,
651 Y., et al. (2020). A neutralizing human antibody binds to the N-terminal domain of the Spike
652 protein of SARS-CoV-2. Science *369*, 650–655. https://doi.org/10.1126/science.abc6952.

653 Collie, S., Champion, J., Moultrie, H., Bekker, L.-G., and Gray, G. (2022). Effectiveness of
654 BNT162b2 Vaccine against Omicron Variant in South Africa. N Engl J Med *386*, 494–496.
655 https://doi.org/10.1056/NEJMc2119270.

656 Dai, L., and Gao, G.F. (2021). Viral targets for vaccines against COVID-19. Nat Rev Immunol
657 *21*, 73–82. https://doi.org/10.1038/s41577-020-00480-0.

658 Espenhain, L., Funk, T., Overvad, M., Edslev, S.M., Fonager, J., Ingham, A.C., Rasmussen, M.,
659 Madsen, S.L., Espersen, C.H., Sieber, R.N., et al. (2021). Epidemiological characterisation of
660 the first 785 SARS-CoV-2 Omicron variant cases in Denmark, December 2021. Euro Surveill
661 *26*. https://doi.org/10.2807/1560-7917.ES.2021.26.50.2101146.

662 Gobeil, S.M.-C., Henderson, R., Stalls, V., Janowska, K., Huang, X., May, A., Speakman, M.,
663 Beaudoin, E., Manne, K., Li, D., et al. (2022). Structural diversity of the SARS-CoV-2 Omicron
664 spike. Molecular Cell, https://doi.org/10.1016/j.molcel.2022.03.028.

665 Golcuk, M., Yildiz, A., and Gur, M. (2021). Omicron BA.1 and BA.2 Variants Increase the
666 Interactions of SARS-CoV-2 Spike Glycoprotein with ACE2. https://doi.org/10.1101/2021.
667 12.06.471377.

668 Grabowski, F., Kochańczyk, M., and Lipniacki, T. (2022). The spread of SARS-CoV-2 variant
669 Omicron with the doubling time of 2.0-3.3 days can be explained by immune evasion. Viruses
670 14(2), 294; https://doi.org/10.3390/v14020294.

671 Hadfield, J., Megill, C., Bell, S.M., Huddleston, J., Potter, B., Callender, C., Sagulenko, P.,
672 Bedford, T., and Neher, R.A. (2018). Nextstrain: real-time tracking of pathogen evolution.
673 Bioinformatics *34*, 4121–4123. https://doi.org/10.1093/bioinformatics/bty407.

674 Harvey, W.T., Carabelli, A.M., Jackson, B., Gupta, R.K., Thomson, E.C., Harrison, E.M.,
675 Ludden, C., Reeve, R., Rambaut, A., COVID-19 Genomics UK (COG-UK) Consortium, et al.
676 (2021). SARS-CoV-2 variants, spike mutations and immune escape. Nat Rev Microbiol *19*, 409–
677 424. https://doi.org/10.1038/s41579-021-00573-0.

678 Hoffmann, M., Kleine-Weber, H., Schroeder, S., Krüger, N., Herrler, T., Erichsen, S.,
679 Schiergens, T.S., Herrler, G., Wu, N.-H., Nitsche, A., et al. (2020). SARS-CoV-2 Cell Entry
680 Depends on ACE2 and TMPRSS2 and Is Blocked by a Clinically Proven Protease Inhibitor. Cell
681 *181*(2):271-280; https://doi.org/10.1016/j.cell.2020.02.052.

682 Hoffmann, M., Krüger, N., Schulz, S., Cossmann, A., Rocha, C., Kempf, A., Nehlmeier, I.,
683 Graichen, L., Moldenhauer, A.-S., Winkler, M.S., et al. (2021). The Omicron variant is highly
684 resistant against antibody-mediated neutralization: Implications for control of the COVID-19
685 pandemic. Cell S0092-8674(21)01495-1. https://doi.org/10.1016/j.cell.2021.12.032.

686 Huang, K., Zhang, Y., Hui, X., Zhao, Y., Gong, W., Wang, T., Zhang, S., Yang, Y., Deng, F.,
687 Zhang, Q., et al. (2021). Q493K and Q498H substitutions in Spike promote adaptation of SARS-
688 CoV-2 in mice. EBioMedicine *67*, 103381. https://doi.org/10.1016/j.ebiom.2021.103381.

689 Humphrey, W., Dalke, A., and Schulten, K. (1996). VMD: visual molecular dynamics. Journal
690 of Molecular Graphics *14*, 33–38, 27–28. .

691 Iketani, S., Liu, L., Guo, Y., Liu, L., Chan, J.F.-W., Huang, Y., Wang, M., Luo, Y., Yu, J., Chu,
692 H., et al. (2022). Antibody evasion properties of SARS-CoV-2 Omicron sublineages. Nature
693 https://doi.org/10.1038/s41586-022-04594-4.

694 Jung, C., Kmiec, D., Koepke, L., Zech, F., Jacob, T., Sparrer, K.M.J., and Kirchhoff, F. (2022).
695 Omicron: what makes the latest SARS-CoV-2 variant of concern so concerning? J Virol
696 jvi0207721. https://doi.org/10.1128/jvi.02077-21.

697 Karim, F., Moosa, M.Y.S., Gosnell, B.I., Cele, S., Giandhari, J., Pillay, S., Tegally, H.,
698 Wilkinson, E., San, J.E., Msomi, N., et al. (2021). Persistent SARS-CoV-2 infection and intra-
699 host evolution in association with advanced HIV infection. medRxiv; doi:
700 https://doi.org/10.1101/2021.06.03.21258228.

701 Korber, B., Fischer, W.M., Gnanakaran, S., Yoon, H., Theiler, J., Abfalterer, W., Hengartner,
702 N., Giorgi, E.E., Bhattacharya, T., Foley, B., et al. (2020). Tracking Changes in SARS-CoV-2

703 Spike: Evidence that D614G Increases Infectivity of the COVID-19 Virus. Cell *182*, 812-
704 827.e19. https://doi.org/10.1016/j.cell.2020.06.043.

705 Krashes, M.J., Koda, S., Ye, C., Rogan, S.C., Adams, A.C., Cusher, D.S., Maratos-Flier, E.,
706 Roth, B.L., and Lowell, B.B. (2011). Rapid, reversible activation of AgRP neurons drives
707 feeding behavior in mice. J Clin Invest *121*, 1424–1428. https://doi.org/10.1172/JCI46229.

708 Lam, S.D., Waman, V.P., Orengo, C., and Lees, J. (2021). Insertions in the SARS-CoV-2 Spike
709 N-Terminal Domain May Aid COVID-19 Transmission. bioRxiv; doi:
710 https://doi.org/10.1101/2021.12.06.471394.

711 Langmead, B., and Salzberg, S.L. (2012). Fast gapped-read alignment with Bowtie 2. Nat
712 Methods *9*, 357–359. https://doi.org/10.1038/nmeth.1923.

713 Letko, M., Marzi, A., and Munster, V. (2020). Functional assessment of cell entry and receptor
714 usage for SARS-CoV-2 and other lineage B betacoronaviruses. Nature Microbiology *5*, 562–
715 569. https://doi.org/10.1038/s41564-020-0688-y.

716 Li, H., Handsaker, B., Wysoker, A., Fennell, T., Ruan, J., Homer, N., Marth, G., Abecasis, G.,
717 Durbin, R., and 1000 Genome Project Data Processing Subgroup (2009). The Sequence
718 Alignment/Map format and SAMtools. Bioinformatics *25*, 2078–2079.
719 https://doi.org/10.1093/bioinformatics/btp352.

720 Liu, L., Iketani, S., Guo, Y., Chan, J.F.-W., Wang, M., Liu, L., Luo, Y., Chu, H., Huang, Y.,
721 Nair, M.S., et al. (2022). Striking antibody evasion manifested by the Omicron variant of SARS-
722 CoV-2. Nature *602*, 676–681. https://doi.org/10.1038/s41586-021-04388-0.

723 Lu, L., Mok, B.W.-Y., Chen, L.-L., Chan, J.M.-C., Tsang, O.T.-Y., Lam, B.H.-S., Chuang,
724 V.W.-M., Chu, A.W.-H., Chan, W.-M., Ip, J.D., et al. (2021). Neutralization of SARS-CoV-2
725 Omicron variant by sera from BNT162b2 or Coronavac vaccine recipients. Clin Infect Dis
726 ciab1041. https://doi.org/10.1093/cid/ciab1041.

727 Maaroufi, H. (2022). The N764K and N856K mutations in SARS-CoV-2 Omicron BA.1 S
728 protein generate potential cleavage sites for SKI-1/S1P protease. 2022.01.21.477298.
729 https://doi.org/10.1101/2022.01.21.477298.

730 Mannar, D., Saville, J.W., Zhu, X., Srivastava, S.S., Berezuk, A.M., Tuttle, K., Marquez, C.,
731 Sekirov, I., and Subramaniam, S. (2022). SARS-CoV-2 Omicron Variant: ACE2 Binding, Cryo-
732 EM Structure of Spike Protein-ACE2 Complex and Antibody Evasion. Science *375*, 760-764.

733 Meng, B., Ferreira, I.A.T.M., Abdullahi, A., Goonawardane, N., Saito, A., Kimura, I.,
734 Yamasoba, D., Gerba, P.P., Fatihi, S., Rathore, S., et al. (2022). SARS-CoV-2 Omicron spike
735 mediated immune escape and tropism shift. Nature *603*, 706–714.

736 Moore, P.L., and Baden, L.R. (2022). Omicron — Decoupling Infection from Severe Disease. N
737 Engl J Med *386*, 1361–1362. https://doi.org/10.1056/NEJMe2201812.

738 Neumann, C.J., and Nuesslein-Volhard, C. (2000). Patterning of the Zebrafish Retina by a Wave
739 of Sonic Hedgehog Activity. Science *289*, 2137–2139. https://doi.org/10.1126/science.
740 289.5487.2137.

741 Oh, E., Zhu, J.-Y., and Wang, Z.-Y. (2012). Interaction between BZR1 and PIF4 integrates
742 brassinosteroid and environmental responses. Nat Cell Biol *14*, 802–809.
743 https://doi.org/10.1038/ncb2545.

744 Planas, D., Veyer, D., Baidaliuk, A., Staropoli, I., Guivel-Benhassine, F., Rajah, M.M.,
745 Planchais, C., Porrot, F., Robillard, N., Puech, J., et al. (2021). Reduced sensitivity of SARS-
746 CoV-2 variant Delta to antibody neutralization. Nature *596*, 276–280.
747 https://doi.org/10.1038/s41586-021-03777-9.

748 Polack, F.P., Thomas, S.J., Kitchin, N., Absalon, J., Gurtman, A., Lockhart, S., Perez, J.L., Pérez
749 Marc, G., Moreira, E.D., Zerbini, C., et al. (2020). Safety and Efficacy of the BNT162b2 mRNA
750 Covid-19 Vaccine. N Engl J Med *383*, 2603–2615. https://doi.org/10.1056/NEJMoa2034577.

751 Pulliam, J.R.C., Schalkwyk, C. van, Govender, N., Gottberg, A. von, Cohen, C., Groome, M.J.,
752 Dushoff, J., Mlisana, K., and Moultrie, H. (2022). Increased risk of SARS-CoV-2 reinfection
753 associated with emergence of the Omicron variant in South Africa. Science; DOI:
754 10.1126/science.abn4947

755 Rath, S.L., Padhi, A.K., and Mandal, N. (2022). Scanning the RBD-ACE2 molecular interactions
756 in Omicron variant. Biochemical and Biophysical Research Communications *592*, 18–23.
757 https://doi.org/10.1016/j.bbrc.2022.01.006.

758 Rau, C., Wisniewski, N., Orozco, L., Bennett, B., Weiss, J., and Lusis, A. (2013). Maximal
759 information component analysis: a novel non-linear network analysis method. Frontiers in
760 Genetics *4*. 28.

761 Riepler, L., Rössler, A., Falch, A., Volland, A., Borena, W., von Laer, D., and Kimpel, J. (2020).
762 Comparison of Four SARS-CoV-2 Neutralization Assays. Vaccines (Basel) *9*, 13.
763 https://doi.org/10.3390/vaccines9010013.

764 Sagulenko, P., Puller, V., and Neher, R.A. (2018). TreeTime: Maximum-likelihood
765 phylodynamic analysis. Virus Evol *4*, vex042. https://doi.org/10.1093/ve/vex042.

766 Sarkar, R., Lo, M., Saha, R., Dutta, S., and Chawla-Sarkar, M. (2021). S glycoprotein diversity
767 of the Omicron variant. medRxiv; doi: https://doi.org/10.1101/2021.12.04.21267284

768 Schmidt, F.I., Lu, A., Chen, J.W., Ruan, J., Tang, C., Wu, H., and Ploegh, H.L. (2016). A single
769 domain antibody fragment that recognizes the adaptor ASC defines the role of ASC domains in
770 inflammasome assembly. The Journal of Experimental Medicine *213*, 771–790.
771 https://doi.org/10.1084/jem.20151790.

772 Schneider, C.A., Rasband, W.S., and Eliceiri, K.W. (2012). NIH Image to ImageJ: 25 years of
773 image analysis. Nat Methods *9*, 671–675. https://doi.org/10.1038/nmeth.2089.

774 Sun, S., Gu, H., Cao, L., Chen, Q., Ye, Q., Yang, G., Li, R.-T., Fan, H., Deng, Y.-Q., Song, X.,
775 et al. (2021). Characterization and structural basis of a lethal mouse-adapted SARS-CoV-2. Nat
776 Commun *12*, 5654. https://doi.org/10.1038/s41467-021-25903-x.

777 Suzuki, R., Yamasoba, D., Kimura, I., Wang, L., Kishimoto, M., Ito, J., Morioka, Y., Nao, N.,
778 Nasser, H., Uriu, K., et al. (2022). Attenuated fusogenicity and pathogenicity of SARS-CoV-2
779 Omicron variant. Nature *603*, 700–705. https://doi.org/10.1038/s41586-022-04462-1.

780 Sztain, T., Ahn, S.-H., Bogetti, A.T., Casalino, L., Goldsmith, J.A., Seitz, E., McCool, R.S.,
781 Kearns, F.L., Acosta-Reyes, F., Maji, S., et al. (2021). A glycan gate controls opening of the
782 SARS-CoV-2 spike protein. Nat Chem *13*, 963–968. https://doi.org/10.1038/s41557-021-00758-
783 3.

784 Tao, K., Tzou, P.L., Nouhin, J., Gupta, R.K., de Oliveira, T., Kosakovsky Pond, S.L., Fera, D.,
785 and Shafer, R.W. (2021). The biological and clinical significance of emerging SARS-CoV-2
786 variants. Nat Rev Genet *22*, 757–773. https://doi.org/10.1038/s41576-021-00408-x.

787 Thoreen, C.C., Kang, S.A., Chang, J.W., Liu, Q., Zhang, J., Gao, Y., Reichling, L.J., Sim, T.,
788 Sabatini, D.M., and Gray, N.S. (2009). An ATP-competitive mammalian target of rapamycin
789 inhibitor reveals rapamycin-resistant functions of mTORC1. J Biol Chem *284*, 8023–8032.
790 https://doi.org/10.1074/jbc.M900301200.

791 Tian, S., Huang, Q., Fang, Y., and Wu, J. (2011). FurinDB: A Database of 20-Residue Furin
792 Cleavage Site Motifs, Substrates and Their Associated Drugs. OPEN ACCESS Int. J. Mol. Sci
793 *12*, 12. https://doi.org/10.3390/ijms12021060.

794 VanBlargan, L.A., Errico, J.M., Halfmann, P., Zost, S.J., Crowe, J.E., Purcell, L.A., Kawaoka,
795 Y., Corti, D., Fremont, D.H., and Diamond, M. (2022). An infectious SARS-CoV-2 B.1.1.529
796 Omicron virus escapes neutralization by several therapeutic monoclonal antibodies. Nature
797 Medicine *28*, 490–495.

798 Viana, R., Moyo, S., Amoako, D.G., Tegally, H., Scheepers, C., Althaus, C.L., Anyaneji, U.J.,
799 Bester, P.A., Boni, M.F., Chand, M., et al. (2022). Rapid epidemic expansion of the SARS-CoV-
800 2 Omicron variant in southern Africa. Nature https://doi.org/10.1038/d41586-021-03832-5.

801 Walls, A.C., Park, Y.-J., Tortorici, M.A., Wall, A., McGuire, A.T., and Veesler, D. (2020).
802 Structure, Function, and Antigenicity of the SARS-CoV-2 Spike Glycoprotein. Cell *181*, 281-
803 292.e6. https://doi.org/10.1016/j.cell.2020.02.058.

804 Wei, C., Shan, K.-J., Wang, W., Zhang, S., Huan, Q., and Qian, W. (2021). Evidence for a mouse
805 origin of the SARS-CoV-2 Omicron variant. J Genet Genomics. *48*, 1111–1121.

806 Wilhelm, A., Widera, M., Grikscheit, K., Toptan, T., Schenk, B., Pallas, C., Metzler, M.,
807 Kohmer, N., Hoehl, S., Helfritz, F.A., et al. (2021). Reduced Neutralization of SARS-CoV-2
808 Omicron Variant by Vaccine Sera and Monoclonal Antibodies. medRxiv; doi:
809 https://doi.org/10.1101/2021.12.07.21267432.

810 Wolter, N., Jassat, W., Walaza, S., Welch, R., Moultrie, H., Groome, M., Amoako, D.G., Everatt,
811 J., Bhiman, J.N., Scheepers, C., et al. (2022). Early assessment of the clinical severity of the
812 SARS-CoV-2 omicron variant in South Africa: a data linkage study. Lancet *399*, 437–446.
813 https://doi.org/10.1016/S0140-6736(22)00017-4.

814 Wrapp, D., Wang, N., Corbett, K.S., Goldsmith, J.A., Hsieh, C.-L., Abiona, O., Graham, B.S.,
815 and McLellan, J.S. (2020). Cryo-EM structure of the 2019-nCoV spike in the prefusion
816 conformation. Science *367*, 1260–1263. https://doi.org/10.1126/science.abb2507.

817 Wrobel, A.G., Benton, D.J., Roustan, C., Borg, A., Hussain, S., Martin, S.R., Rosenthal, P.B.,
818 Skehel, J.J., and Gamblin, S.J. (2022). Evolution of the SARS-CoV-2 spike protein in the human
819 host. Nat Commun *13*, 1178. https://doi.org/10.1038/s41467-022-28768-w.

820 Xia, S., Chan, J.F.-W., Wang, L., Jiao, F., Chik, K.K.-H., Chu, H., Lan, Q., Xu, W., Wang, Q.,
821 Wang, C., et al. (2022). Peptide-based pan-CoV fusion inhibitors maintain high potency against
822 SARS-CoV-2 Omicron variant. Cell Res *32*, 404–406. https://doi.org/10.1038/s41422-022-
823 00617-x.

824 Yamasoba, D., Kimura, I., Nasser, H., Morioka, Y., Nao, N., Ito, J., Uriu, K., Tsuda, M.,
825 Zahradnik, J., Shirakawa, K., et al. (2022). Virological characteristics of SARS-CoV-2 BA.2
826 variant. 2022.02.14.480335. https://doi.org/10.1101/2022.02.14.480335.

827 Yurkovetskiy, L., Wang, X., Pascal, K.E., Tomkins-Tinch, C., Nyalile, T.P., Wang, Y., Baum,
828 A., Diehl, W.E., Dauphin, A., Carbone, C., et al. (2020). Structural and Functional Analysis of
829 the D614G SARS-CoV-2 Spike Protein Variant. Cell *183*, 739-751.e8.
830 https://doi.org/10.1016/j.cell.2020.09.032.

831 Zhang, J., Cai, Y., Lavine, C.L., Peng, H., Zhu, H., Anand, K., Tong, P., Gautam, A., Mayer,
832 M.L., Rits-Volloch, S., et al. (2022). Structural and functional impact by SARS-CoV-2 Omicron
833 spike mutations. Cell Reports 110729. https://doi.org/10.1016/j.celrep.2022.110729.

834 Zhang, L., Li, Q., Liang, Z., Li, T., Liu, S., Cui, Q., Nie, J., Wu, Q., Qu, X., Huang, W., et al.
835 (2021). The significant immune escape of pseudotyped SARS-CoV-2 Variant Omicron. Emerg
836 Microbes Infect 1–11. https://doi.org/10.1080/22221751.2021.2017757.

837 Zhao, H., Lu, L., Peng, Z., Chen, L.-L., Meng, X., Zhang, C., Ip, J.D., Chan, W.-M., Chu, A.W.-
838 H., Chan, K.-H., et al. (2021). SARS-CoV-2 Omicron variant shows less efficient replication
839 and fusion activity when compared with delta variant in TMPRSS2-expressed cells. Emerging
840 Microbes & Infections *0*, 1–18. https://doi.org/10.1080/22221751.2021.2023329.

841

Fig. 1

Pastorio, Zech *et al.*

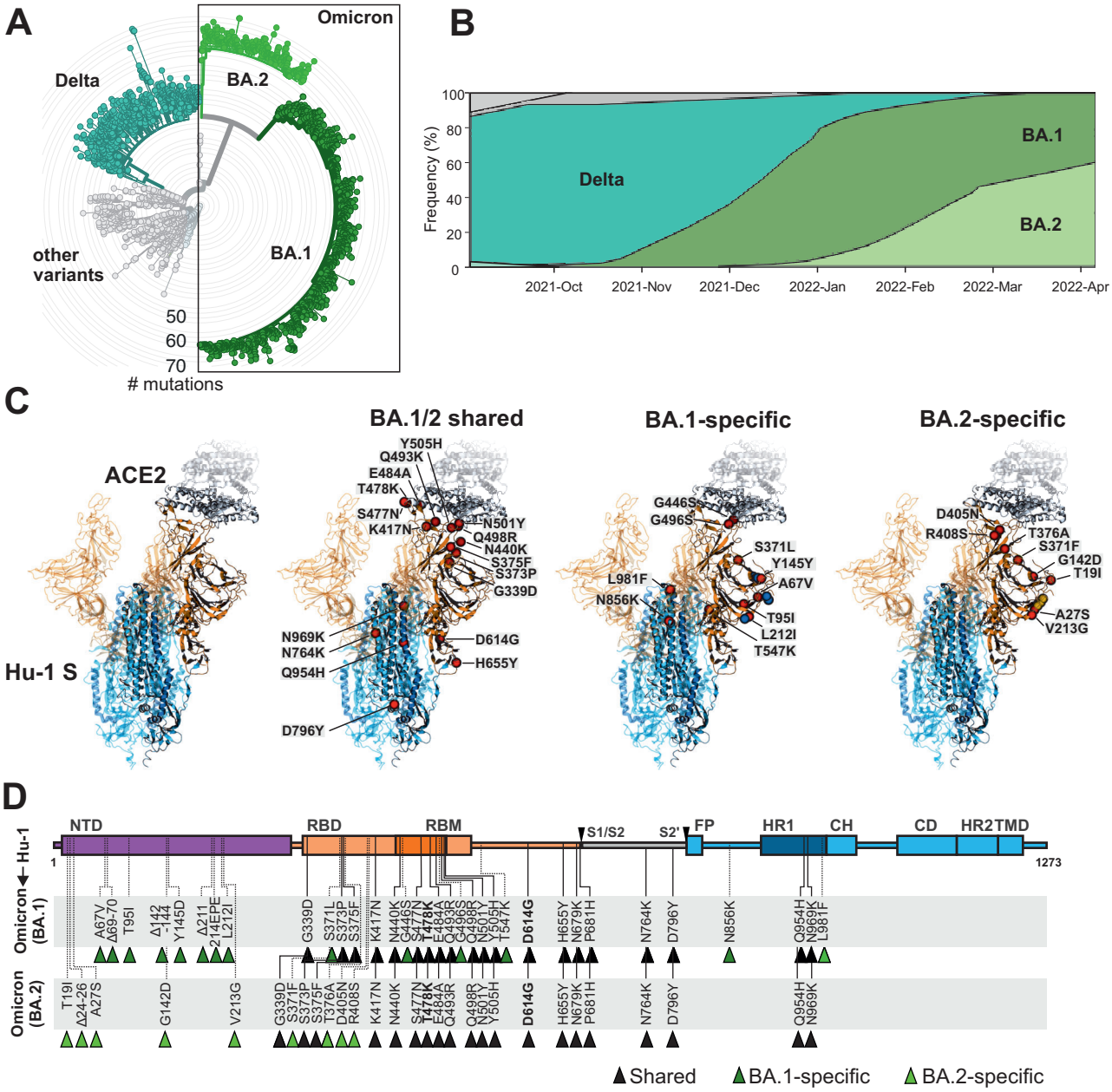

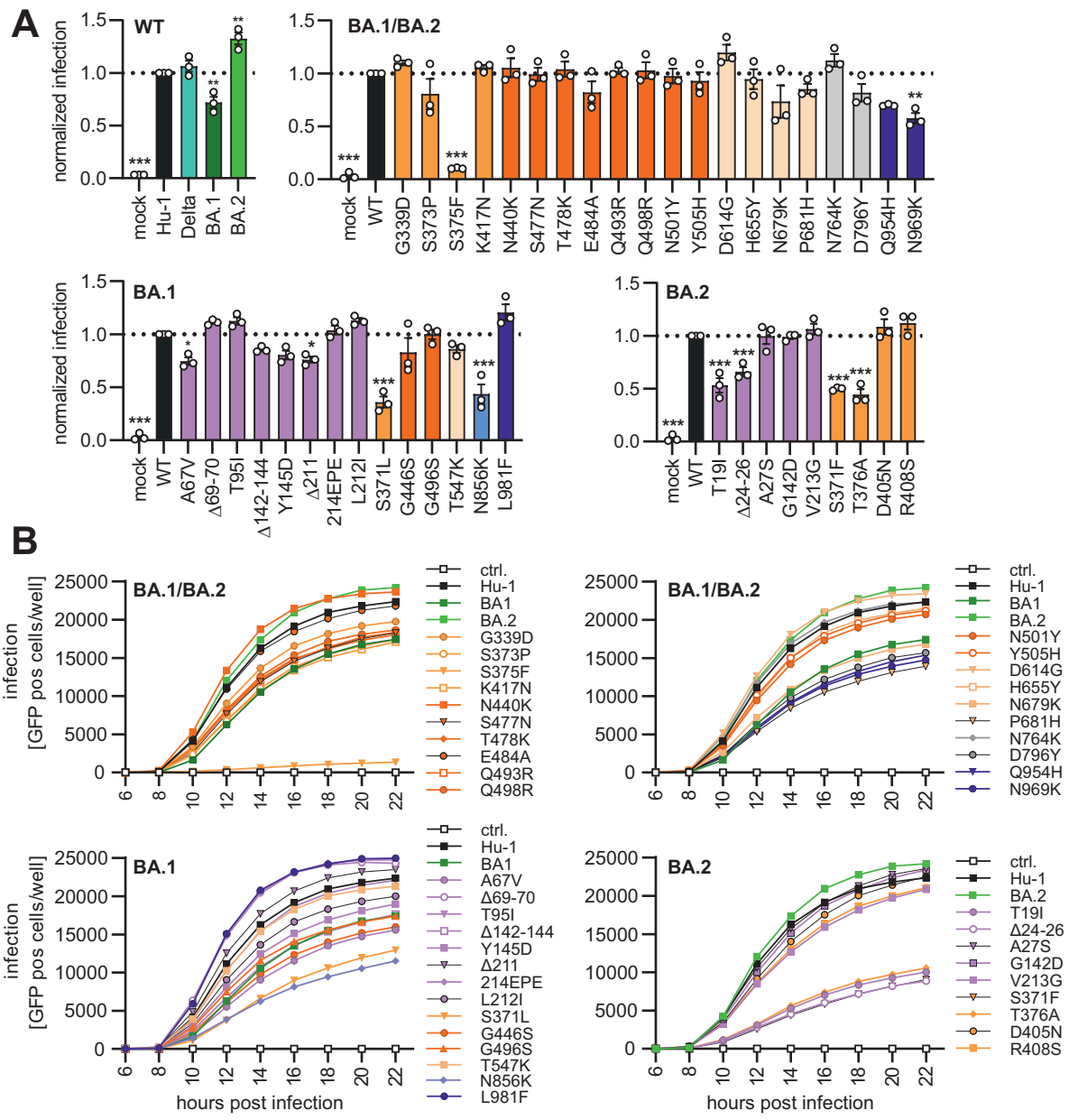

Fig. 3

Pastorio, Zech *et al.*

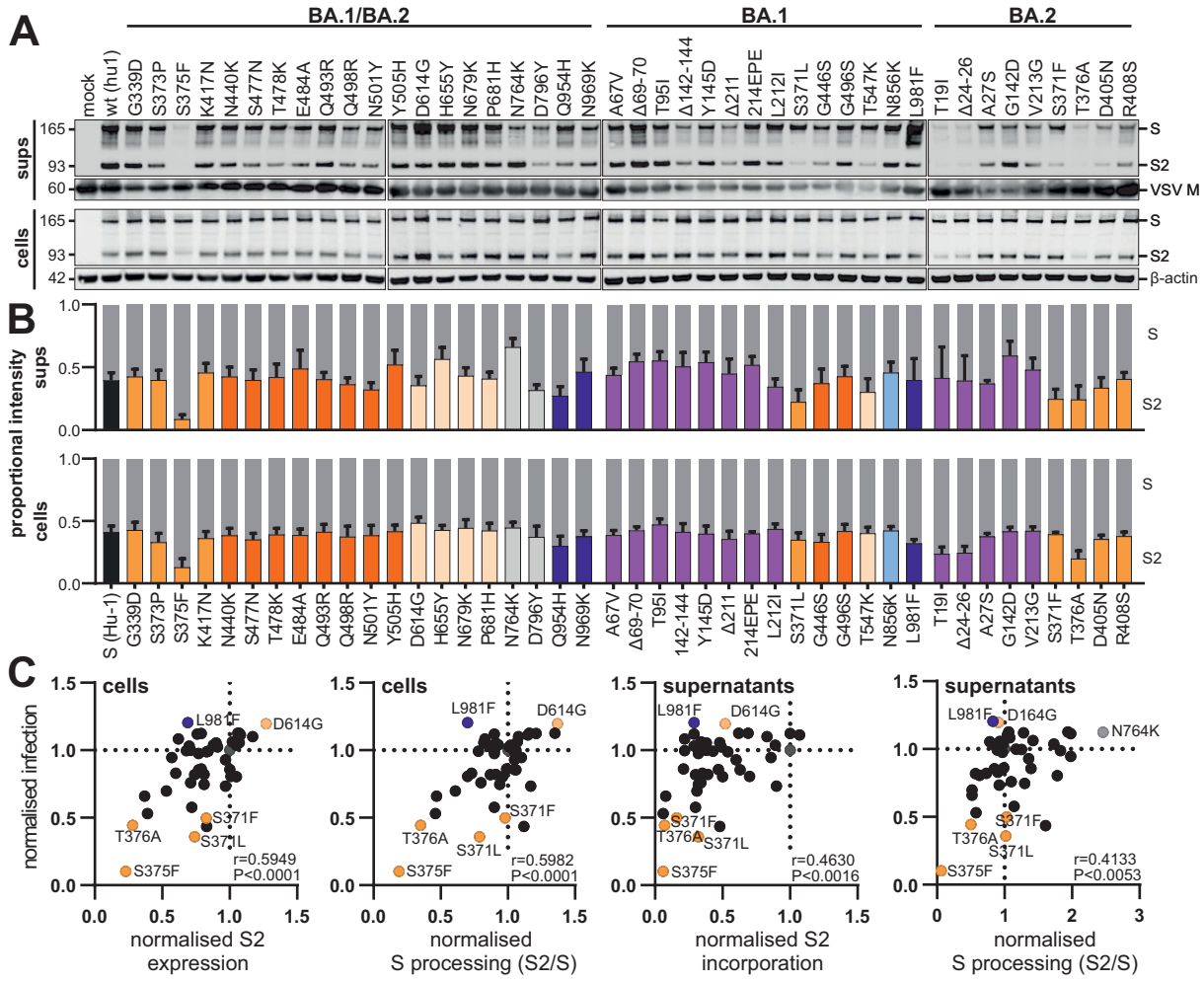

Fig. 4

Pastorio, Zech *et al.*

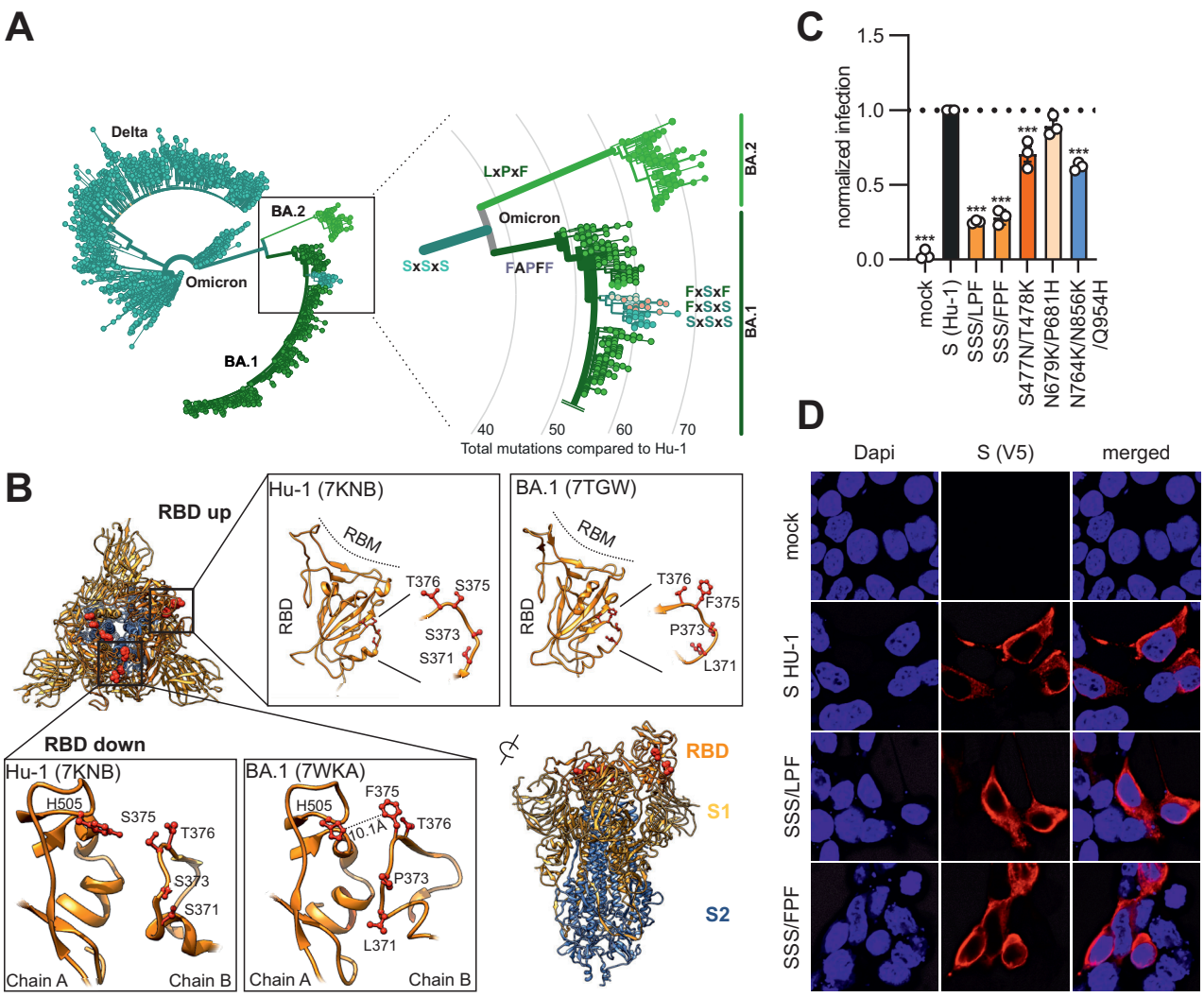

Fig. 5

Pastorio, Zech *et al.*

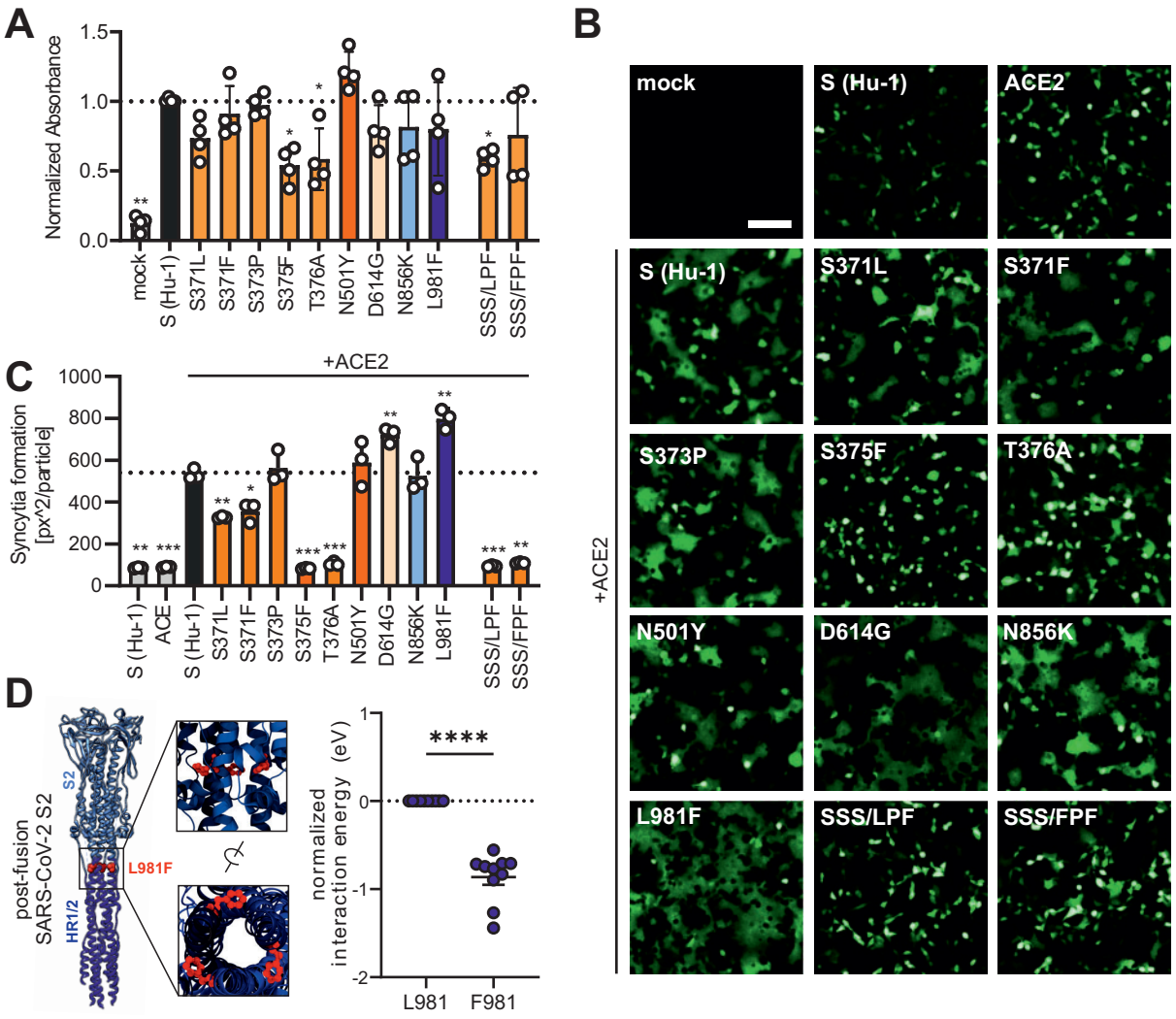

Fig. 6

Pastorio, Zech *et al.*